MIPSGAL v3.0 Data Delivery Description Document (29 August 2008)

Sean J. Carey, Donald R. Mizuno, Kathleen Kraemer, Sachin Shenoy, Alberto Noriega-Crespo, Stephan D. Price, Roberta Paladini, Tom Kuchar

Delivery History

18 July 2008 v3.0 Delivery of 24 μm for -68° < *l* < 69º, |*b*| < 1°, -8° < *l* < 9º, |*b*| < 3°

16 October 2007 v2.0 Delivery of 24 μm mosaics for 292° < *l* < 350° and 10º < *l* < 69º, |*b*| < 1°

17 September 2007 v1.0 Delivery of 24 μm mosaics for 10º < *l* < 69º, |*b*| < 1°

Contents of the third delivery

In the third release, we provide mosaics for all of the survey region including the Galactic center area mapped by PID 20414. $|b| < 1^\circ$ is covered for $-68^\circ < l < 69^\circ$ and $|b| < 3^\circ$ is covered for $-8^\circ < l < 9^\circ$. The mosaics from the regions covered in the 1st and 2nd deliveries are unchanged. In this release, we provide the standard deviation (std) mosaics for estimating the uncertainties in the data instead of the uncertainty mosaics. We have found the std mosaics to be a more reliable estimate of the errors in surface brightness and photometry.

Contents of the second delivery

In the second release, we provide mosaics of ~80% of the survey region. The latitude coverage of the mosaics is complete from $l = 350^\circ$ to 298° and from $l = 10^\circ$ to 63°. The mosaics from the 1st delivery are included unchanged as part of this delivery. As the l = 10 to 63 mosaics are unchanged from the first delivery, users accessing those data from the Spitzer popular products site will find them in http://data.spitzer.caltech.edu/popular/mipsgal/2007_Sep_25/. The mosaics at larger distances from $l = 0^\circ$ are partially covered due to the scanning strategy employed in the survey. The coverage for $|b| > 0.9^\circ$ is also partial for about 15% of the mosaics as the coverage was limited by the scan length quantization in the MIPS AOT and the map angle constraints of the Spitzer orbit.

In addition to the mosaics, corresponding uncertainty images, coverage maps and masks are included. This release is comprised of 239 individual mosaics amounting to 9.6 Gb of image data with an additional 36.0 Gb of corresponding uncertainty and coverage images and mask

cubes. Future deliveries will provide the 24 μm mosaics for $|l| < 10^{\circ}$, mosaics at 70 μm and source lists at both 24 and 70 μm.

Contents of first delivery

In this initial release, we provide 24 μm mosaics of ~40% of the survey region. The latitude coverage of the mosaics is complete out to $l = 63^{\circ}$. The mosaics at larger longitudes are partially covered due to the scanning strategy employed in the survey. The coverage for $|b| > 0.9^{\circ}$ is also partial for about 15% of the mosaics as the coverage was limited by the scan length quantization in the MIPS AOT and the map angle constraints of the Spitzer orbit.

In addition to the mosaics, corresponding uncertainty images, coverage maps and masks are included. This release is comprised of 117 individual mosaics amounting to 4.7 Gb of image data with an additional 17.6 Gb of corresponding uncertainty and coverage images and mask cubes.

All enhanced MIPSGAL products are available from the NASA/IPAC Infrared Science Archive (IRSA; http://irsa.ipac.caltech.edu/SPITZER/MIPSGAL) and the Spitzer Science Center (http://data.spitzer.caltech.edu/popular/). The raw and basic calibrated data for all MIPSGAL observations are available using Leopard (http://ssc.spitzer.caltech.edu/propkit/spot/).

Quick facts on 24 μm mosaics

Resolution: 6 arcseconds
Sampling: 1.25 arcseconds
Point Source Sensitivity: 1.7 mJy (5 σ)
Saturation level: 1700 MJy/sr (extended source), ~2 Jy (point source)
Average Diffuse Signal to Noise:

- for pixels < 10 MJy/sr: 27.5
- for pixels > 10 MJy/sr < 20 MJy/sr: 48.7
- for pixels > 20 MJy/sr < 50 MJy/sr: 88.9
- for pixels > 50 MJy/sr < 100 MJy/sr: 158.8
- for pixels > 100 MJy/sr < 200 MJy/sr: 259.1
- for pixels > 200 MJy/sr < 1000 MJy/sr: 407.6
- for pixels > 1000 MJy/sr: 441.6

Introduction to MIPSGAL project

MIPSGAL is a survey of the inner 278 square degrees of the Galactic plane at 24 and 70 μm using the Multiband Imaging Photometer System (MIPS; Rieke et al. 2004) aboard the Spitzer Space Telescope (Werner et al. 2004). The intent of the MIPSGAL survey is to provide a well sampled, uniform dataset to the community to explore high mass star formation and the physics of interstellar dust in the Milky Way Galaxy. Future data releases will provide the remainder of the mosaics at 24 μm, mosaics at 70 μm, source lists at 24 and 70 μm and source subtracted mosaics.

MIPSGAL consists of two distinct Spitzer observing programs. The cycle-2 program (Program ID 20597, Sean Carey principal investigator) mapped the regions $10° < l < 62°$ and $298° < l < 350°$ for $b < |1°|$. The cycle-3 program (MIPSGAL II; program ID 30594, Sean Carey principal investigator) extended the map to $4° < l < 10°$ and $350° < l < 356°$ for $b < 1°$ and covered the region $|l| < 5°$ for $1 < |b| < 3°$. The region about the Galactic center was previously mapped by program 20414 (Farhad Yusef-Zadah principal investigator). The coverage of the MIPSGAL observations is shown in Figure 1. The MIPSGAL observations were spread over three observing campaigns (October 2005, April 2006 and October 2006). The data in this release are from the first observing campaign, but the data reduction strategy and methods apply to all MIPSGAL data.

The MIPSGAL region was observed using the MIPS fast scan Astronomical Observing Template (AOT). Each position was covered by two overlapping scan legs at 24 μm for a minimum coverage of ten samples per position. For much of the survey region, the overlapping scans were in opposite direction to minimize the effects of bright source latents in the data. For regions within 15 degrees of the Ecliptic plane, the overlapping coverages were separated by 3-9 hours to permit the identification and rejection of main belt asteroids. The current data product only has previously known or bright asteroids removed.

Mosaics of region covered

Figure 2 displays the mosaics comprising this 1st quadrant (September 2007 delivery) tiled together in Galactic coordinates. The majority of the survey region has complete coverage for $|b| < 1°$; however, the region between 35° and 45° has slightly less latitude coverage as shown in Figure 2. Some of the bright regions such as M17 have their cores saturated. Figure 3 displays the 4th quadrant mosaics which make up this delivery. The region from 320° to 331° has slightly less than nominal latitude coverage due to the scan length quantization.

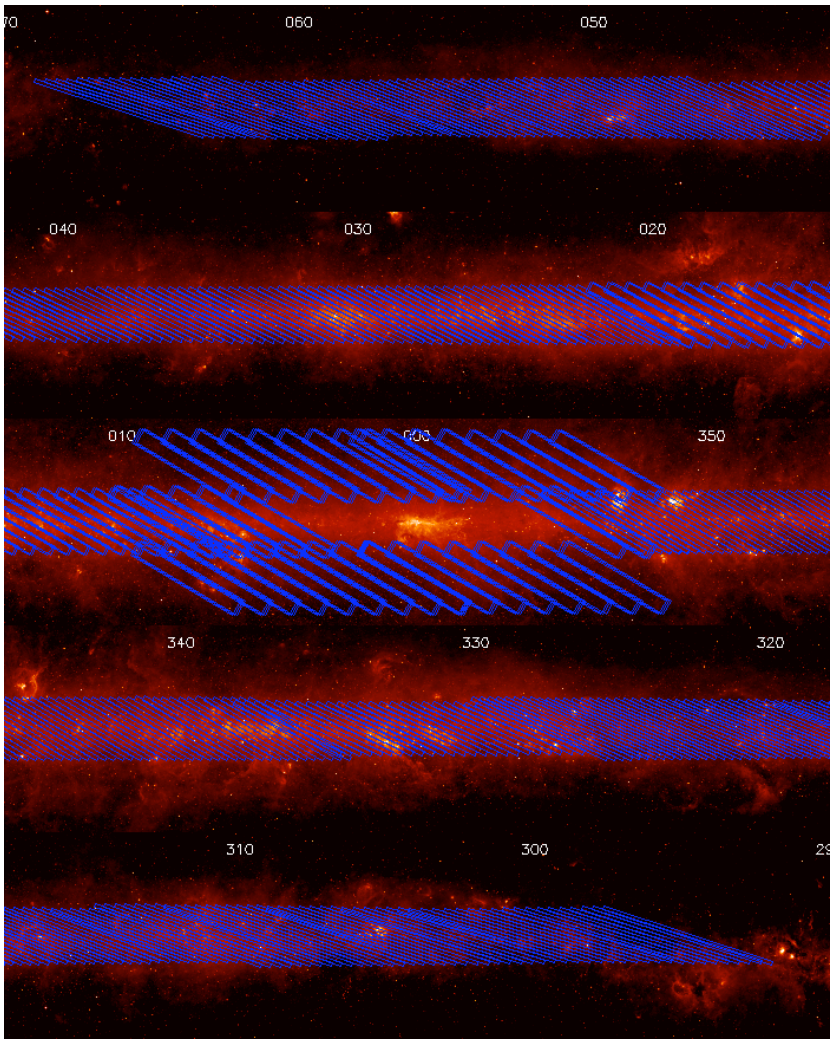

Figure 1: Coverage of MIPSGAL survey observations overlaid on MSX 8.3 μm image. The panels cover Galactic longitudes from 70° to 290° and latitudes from -3.5° to 3.5°.

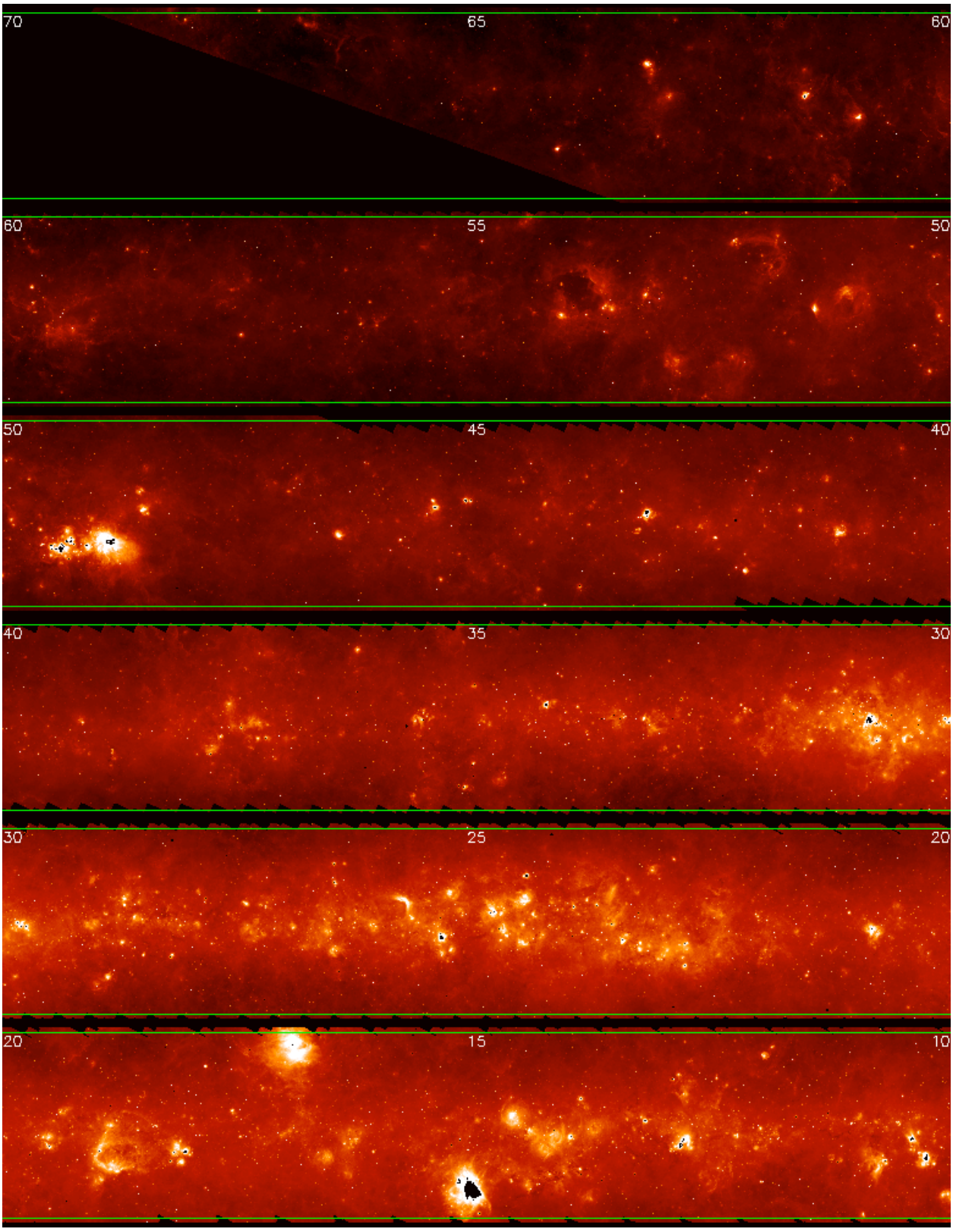

Figure 2: 24 µm mosaics comprising *l* > 10° quadrant data in this delivery. Each panel of the figure is 10° x 2.2°. The Galactic longitude is marked every 5°. The green lines indicate *b*= +1° and -1°.

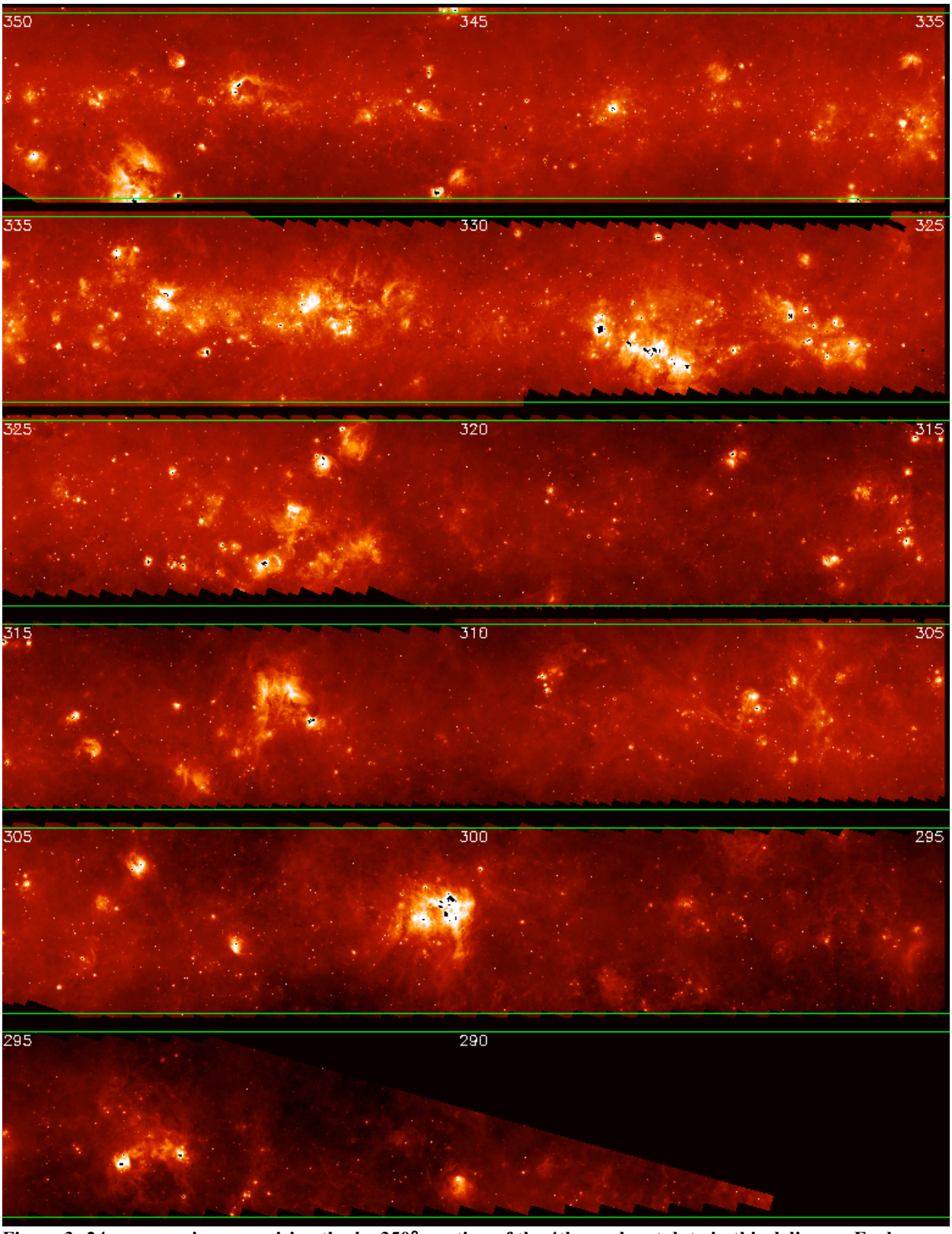

Figure 3: 24 µm mosaics comprising the $l < 350°$ portion of the 4th quadrant data in this delivery. Each panel of the figure is 10° x 2.2°. The Galactic longitude is marked every 5°. The green lines indicate $b = +1°$ and -1°.

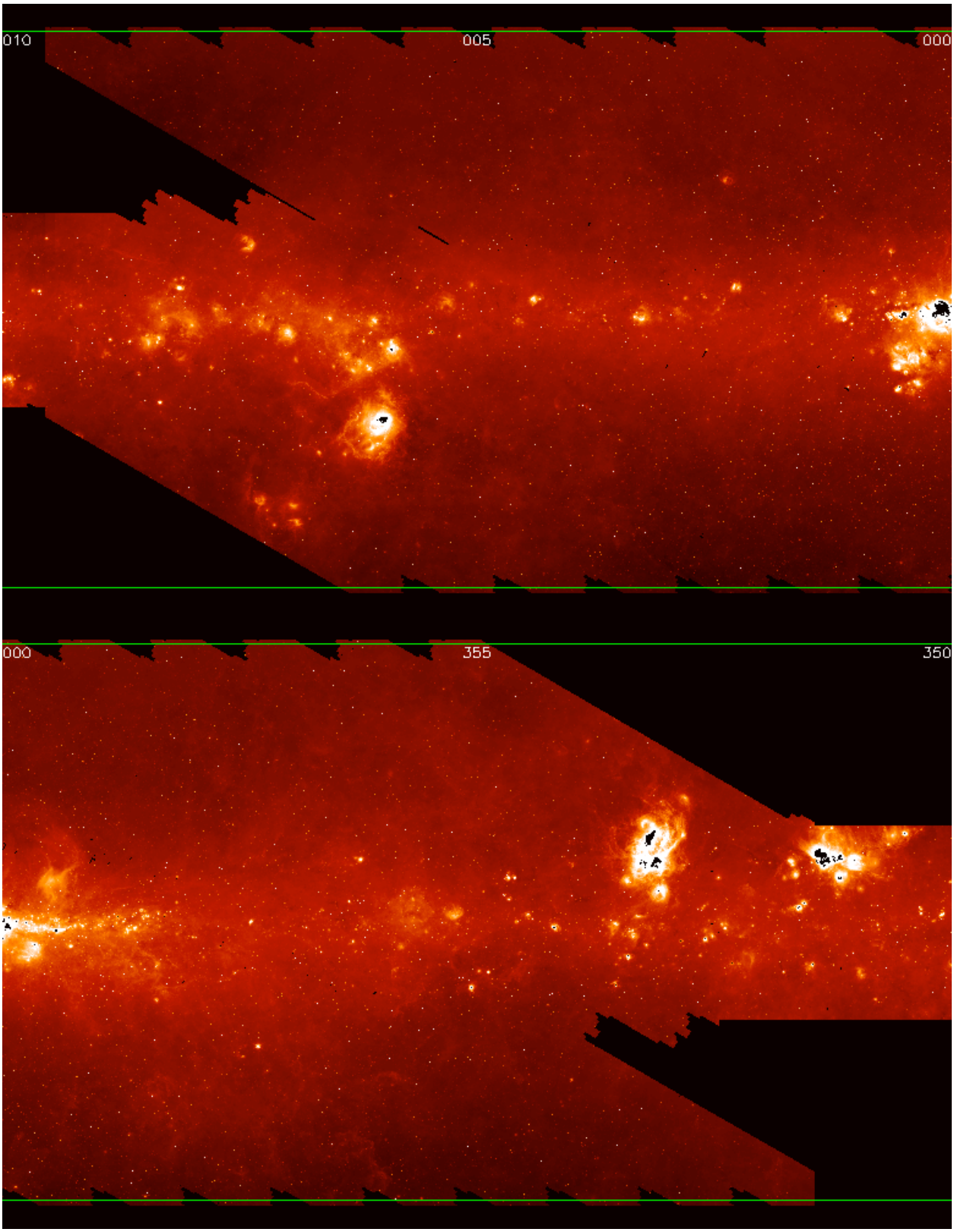

Figure 4: 24 μm mosaics comprising -10° < *l* < 10° data in this delivery. Each of the two panels of the figure is 10° x 6.2°. The Galactic longitude is marked every 5°. The green lines indicate *b*= +3° and -3°.

Description of data products

Mosaics

After pre-processing the basic calibrated data (BCDs) (Mizuno et al. 2008, and as summarized below), the MOPEX package (Makovoz et al. 2006) is used to generate the image plates. The 24 μm mosaics are 1.1º x 1.1º in size and are spaced on one degree centers. The images are in units of surface brightness (MJy/sr) and use the standard MIPS calibration and zero point (Engelbracht et al. 2007). A model of the Zodiacal light (Kelsall et al. 1998) has been subtracted from the input data before coaddition. Pixels without data contain IEEE floating point NaNs. The images are sampled on 1.25 arcsec centers. The image coordinates are Equatorial J2000 and a tangent projection is used in constructing the mosaic. A rotation angle is applied (non-zero CROTA2 keyword) such that the images are aligned in Galactic coordinates. This is strictly true for the center of each mosaic and holds true for all practical purposes for the entirety of each plate. The astrometric information is encoded in each mosaic header following the format recommendations of Calabretta and Greisen (2002). The mosaic headers include information on the processing steps applied as well as a list of the request keys of AORs contributing data to the mosaic. The number of AORs used in the mosaic is given by the NAOR keyword. The AOR request keys are provided by the AORKEY## keywords (where ## is an integer, 00, 01, …). The start time of each AOR used is contained in the AORTIM## keywords. The processing version of the mosaics in this delivery is noted in the keyword, VERSION, and is 1.1 for this release. An example of a mosaic header is given in the appendix.

In addition to the astrometric and photometric keywords, including the flux conversion factor (FLUXCONV) and gain (GAIN), the mosaic headers include a set of Boolean flags to indicate whether various artifact mitigation steps were performed on the input BCDs. Corrections for array droop, jailbars, dark latents and bright latents are indicated by the DROOP, JAILBAR, DARKLAT and BRITELAT keywords. Removal of a bias pattern in the BCDs is indicated by the WASHBRD keyword (as the bias pattern has a washboard appearance in the BCDs). Overlap correction is indicated by the OVERLAP keyword. Flagging of glints due to bright sources on the edge of the array and bright, known asteroids is indicated by the EDGEMASK and ASTRDMSK keywords.

The image header also includes various statistics such as the minimum and maximum data values, keywords DATAMIN and DATAMAX, respectively. The input pixel coverage statistics are included as they are for the coverage mosaics (see the following subsection). The number in the input BCDs which are hard saturated and percentage of mosaic pixels which are flagged as hard saturated are given in the keywords, NHARDALL and PHARDSAT. The keywords, NSOFTSAT and PSOFTSAT provide the analogous quantities for soft saturation.

Uncertainty mosaics

As part of the mosaic process, standard deviation (std) mosaics in units of surface brightness are also generated. The std mosaic headers include the same astrometric information as the mosaics and the uncertainties are in units of MJy/sr. The std mosaics are formed from the standard deviation of the interpolated input BCD pixel stacks which are area weighted and coadded to form the output mosaic pixels. The noise of the mosaics scales as the square root of the coverage and is generally dominated by the Poisson noise of the emission of the Galactic plane. The noise for bright point sources is higher (2-5×) than Poisson as the slight misregistration of the input BCDs causes most of the scatter in the pixel stack for bright pixels.

Coverage mosaics

The coverage mosaics indicate the number of input image pixels coadded for each mosaic pixel. The mosaicking procedure weights each input pixel by its area overlap with an output pixel; therefore, the coverage can include fractions of a pixel. On average, 12 input data samples contribute to each output mosaic pixel. The coverage is highly position dependent and varies from a nominal minimum of 9-10 up to 18-19 for the regions where edges of scans overlap. The coverage mosaics also include the same astrometric information as the image mosaics. The keywords COVRGMAX, COVGRMIN and COVRGMN, give the minimum, maximum and mean coverage of all pixels with non-zero coverage, respectively. NCOVREG0 provides the number of pixels with zero coverage.

Mask mosaic cubes

The mask cubes display the number of input samples that were flagged as problematic for each output mosaic pixel. All samples that were flagged as problematic were not used to create the mosaics. Positions that have no good data are filled with NaN in the output mosaic. Therefore, the mask cubes are complementary to the coverage mosaics and indicate why the coverage for a given pixel is less than optimal. Seven states are indicated in the mosaic mask. The first plane indicates input pixels which are hard saturated. The second plane indicates BCD pixels which are affected by stray light from a bright source on the edge of or just off the array. The third plane flags input pixels which cannot be flat-fielded. The fourth plane displays pixels which have been edited out due to known asteroids or asteroids that were partially removed by the outlier rejection step for positions observed at multiple epochs ($10° < l < 20°$). The fifth plane indicates data which are flagged as bad in the MIPS pmask (see the MIPS Data Handbook for more details; http://ssc.spitzer.caltech.edu/mips/dh/). The sixth plane flags BCD pixels which are soft saturated. The final bit plane displays regions with missing input pixels due to downlink problems.

The mask cubes have the same astrometric information as the image mosaics. The photometry of regions with some saturated samples will probably be less reliable. Faint sources or structure in regions with known stray light should be investigated further to ensure their validity.

Brief description of processing pipeline and mosaic generation

The mosaics were generated by regridding and coadding the individual data collection events (DCEs) after the raw data was processed through a 24 μm pipeline that we developed. We mosaicked the pipeline processed images using the MOPEX software supplied by the SSC. The mosaic processing applied temporal outlier rejection to remove radiation hits and other transients before coaddition. Data previously masked as bad due to saturation, non-linearity, etc. were also omitted through the application of the appropriate mask files.

The 24 μm pipeline to process raw data into BCDs consists of two parts. The first part applies basic calibrations such as bias subtraction, droop correction linearization and flat-fielding. This pipeline is based on the SSC pipeline but has several enhancements in saturated pixel handling and droop correction. These enhancements are particularly important for the high signal and background fluxes in the Galactic plane.

After processing into BCDs, several steps of artifact mitigation were applied to the BCDs. Long term latents of both the bright and dark variety were identified from time ordered stacks of BCDs and removed. Short term latents from fainter, but still bright sources were identified by identifying triggering sources and fitting a time dependent latent model to the affected pixels. Jailbars and other bright source effects such as image level jumps were identified and removed by a variety of procedures. Artifacts that could not be reliably mitigated were flagged and an appropriate bit was set in the mask corresponding to each BCD. As a final step prior to mosaicking, an estimate of the Zodiacal light was removed and DC offsets between overlapping BCDs were corrected by performing a global overlap correction. The pipeline processing and artifact mitigation are described in detail by Mizuno et al. (2008).

The mosaics were inspected visually to identify residuals due to incomplete rejection of asteroids, stray light features, and discontinuities in the row/column containing a bright source. Typically, these residuals are present in only a handful of the BCDs that have been coadded. The problematic data are identified and appropriately masked. The mosaics are then regenerated without the artifacts. The resulting mosaics are then inspected by a different member of the MIPSGAL team. A future data release will include region-of-interest files produced by this quality assurance inspection. These region-of-interest files will indicate the position and extent of any remaining known low level artifacts in the mosaics.

Astrometric accuracy

Unlike IRAC images, no pointing refinement is performed on the MIPS BCDs. The pointing accuracy of the mosaics is the result of the combined effect of the blind pointing accuracy of Spitzer (~1 arcsec rms) and the inability of the MIPS Cryogenic Scan Mirror Mechanism to return to the same zero point (~0.5 arcsec). An assessment of the astrometric accuracy is given by matching positions of point sources in the 24 μm mosaics with the sources at 8 μm from the GLIMPSE Point Source Catalog (http://data.spitzer.caltech.edu/popular/glimpse/20070416_enhanced_v2/source_lists/). Figure 5

displays the offset between source matches at 24 and 8 μm. The median offset between 24 μm source and its 8 μm counterpart is 0.85 arcseconds which is in keeping with the two effects mentioned previously mentioned. GLIMPSE sources were matched by finding the nearest GLIMPSE source within a 5 arcsecond search radius. A straight positional association was used without any flux comparison. The red curve shows the estimated random matches as a function of distance between sources assuming an average source density of 33225 sources / square degree for GLIMPSE.

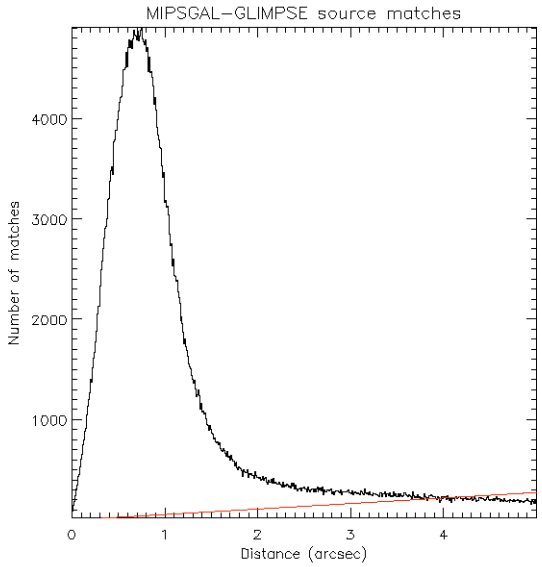

Figure 5: Histogram of positional offset between MIPSGAL 24 μm point sources and corresponding 8 μm point sources from GLIMPSE. The red line is the expected number of random associations per unit distance.

Photometric accuracy

We checked the photometric accuracy of our data reduction by comparing the surface brightness of the data to MSX 21.3 μm measurements and comparing the fluxes of point sources of known spectral types (AV and KIII stars) to flux measurements from GLIMPSE. Figure 6 displays the pixel to pixel correlation between MIPSGAL data smoothed to the same resolution as MSX 21.3 μm data of M16. Each dataset was color corrected using a correction appropriate for massive star forming regions (Flagey private communication). The pixel to pixel relation is well matched by the relationship

$$\frac{MIPSGAL}{MSX} = \left(\frac{\lambda_{MIPSGAL}}{\lambda_{MSX}} \right)^{1.5}$$

where $\lambda_{MIPSGAL}$ and λ_{MSX} are the isophotal wavelengths of MIPS 24 μm and MSX Band E, respectively and the relationship is appropriate for the spectral energy distribution of dust in a massive star forming region. The departure of the data from the model for surface brightness starting at 1000 MJy/sr and more significant for 1500 MJy/sr for MIPSGAL is most likely due to

compact sources which will have a different spectral energy distribution that the ISM. At 1700 MJy/sr, the plot clearly indicates that the MIPSGAL data is saturated.

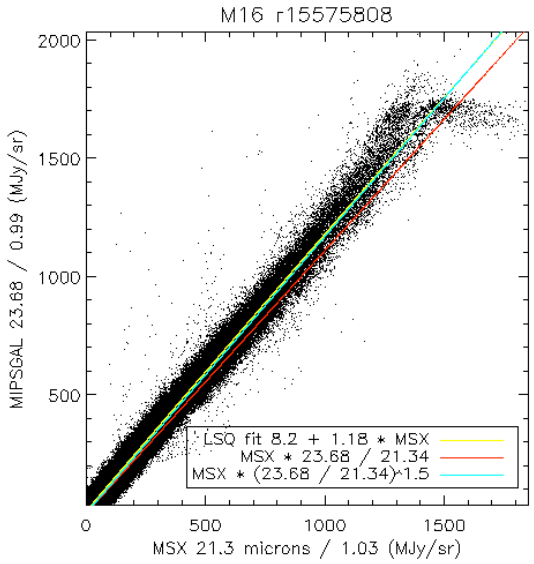

Figure 6 : Pixel to pixel scatter plot of color corrected MSX 21.3 μm surface brightness as compared to color corrrected 23.68 μm MIPSGAL surface brightness for the region around M16.

As a quick check of the point source photometry that can be derived from this image product, we measured the flux densities at 24 μm of a set of stars of known spectral type (K0III-K2III and A0V-A2V) and with flux densities from 2MASS and GLIMPSE. The APEX source extractor (Makovoz & Marleau 2005) provided by the SSC was used on the mosaics. The fit residuals were inspected by eye and any sources with fit residuals not consistent with the noise of the data were rejected. In general, the fits were good despite a fair amount of background structure in the images. Figure 7 displays the 24 μm image of HD 166290 and the residuals of the source fit.

We predicted the MIPSGAL flux densities for the stars using the GLIMPSE 8.0 μm measurement and a spectral template of a well characterized star of the same spectral type. The spectral templates used were from Engelke et al. (2006) for the K giants and Cohen et al. (2003) for the A dwarfs. In converting the flux densities to magnitudes, we used zero magnitude flux densities of 64.1 (Laine et al. 2006) and 7.17 Jy (Engelbracht et al. 2007) for [8.0] and [24.0], respectively. Figure 8 plots the color excess ($E_{[8]-[24]}$) of the measured photometry compared to the model prediction for the 27 stars with spectral types corresponding to the available spectral templates and good photometry in MIPSGAL and GLIMPSE 8 μm. Most of the stars have photometry in good agreement with the model, although four stars have significant excesses (>0.2 mag) at 24 μm. Three of the excess stars are A dwarfs and most likely have debris disks. The fourth star HD 168701 is an eclipsing variable with a secondary of unknown spectral type (Malkov et al. 2006). The average excess for the stars with $E_{[8]-[24]} > -0.2$ is -0.03. This offset has also been noted by the SAGE legacy team using a similar analysis (Meixner 2007; note that they plot measured-predicted, thus the sign of the offset is reversed). The offset is within the cross-calibration error (5%) between IRAC and MIPS.

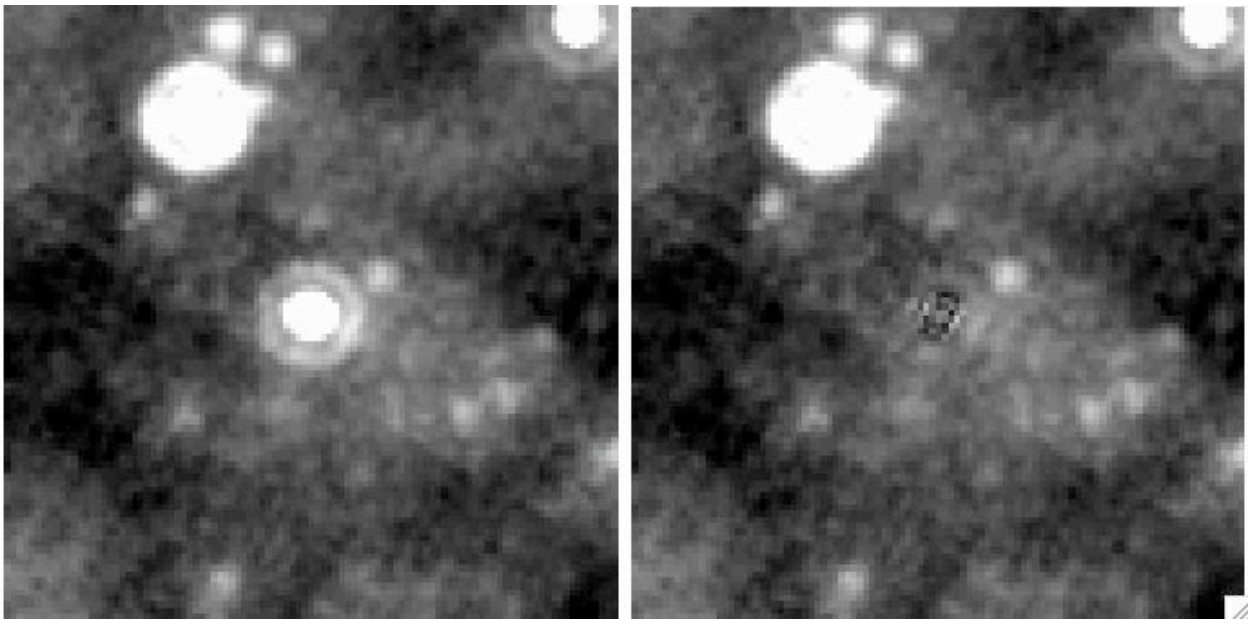

Figure 7: HD 166290 (left) and residual image after source fit (right). The image stretch is the same in both panels. The stripe pattern of the residual is due to the oversampling of the mosaic and the Poisson noise of the individual samples. A level jump between scanlegs is visible just below HD 166290.

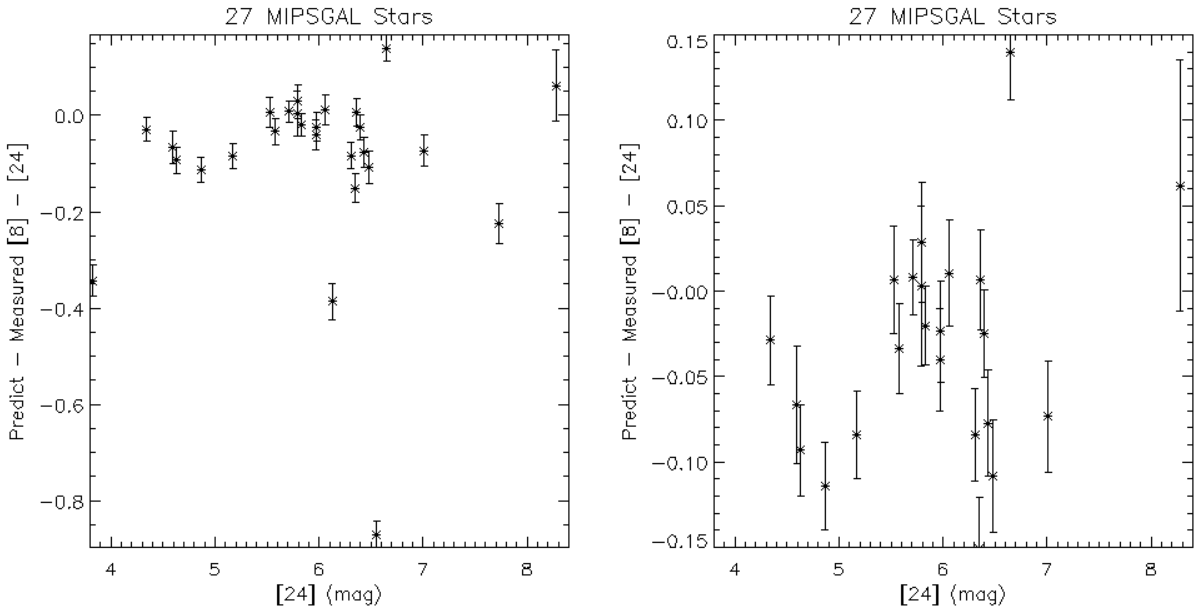

Figure 8: [8]-[24] color excess between GLIMPSE 8.0 μm and 24 μm predicted color and measured GLIMPSE 8.0 and MIPSGAL 24 μm color. Left panel shows all stars with template predictions. Right panel shows all |color excess| < 0.15.

Remaining artifacts

Despite the artifact mitigation applied and the remosaicking of the data after an initial quality assessment and masking of artifacts in the BCDs, some low level artifacts do remain in the mosaics. The remaining artifacts are usually due to bright sources and are mostly aligned parallel or perpendicular to the scan direction. The in-scan direction is approximately 70 degrees counterclockwise from Galactic north (the positive y-direction in the mosaics). We present examples of the known remaining artifacts to aid users in their analysis and to prevent identification of artifacts as interesting "sources".

Low-level Pattern Noise

In all of the data but particularly for the lower background regions, there exists pattern noise which presents itself as high-frequency in-scan stripes (that is the variation is along the in-scan direction) as shown in Figure 9. The amplitude of these stripes is about 0.05 MJy/sr. We verified that the stripes are in the data and not an aliasing artifact of the mosaicking process by generating mosaics with different orientations with respect to the scan direction and different pixel sizes. In all test mosaics, the stripes were present. The stripes do not maintain a constant amplitude in the cross-scan direction and appear to vary temporally with an ill-defined periodicity. Their effect on photometry of either point or extended sources is to increase the noise.

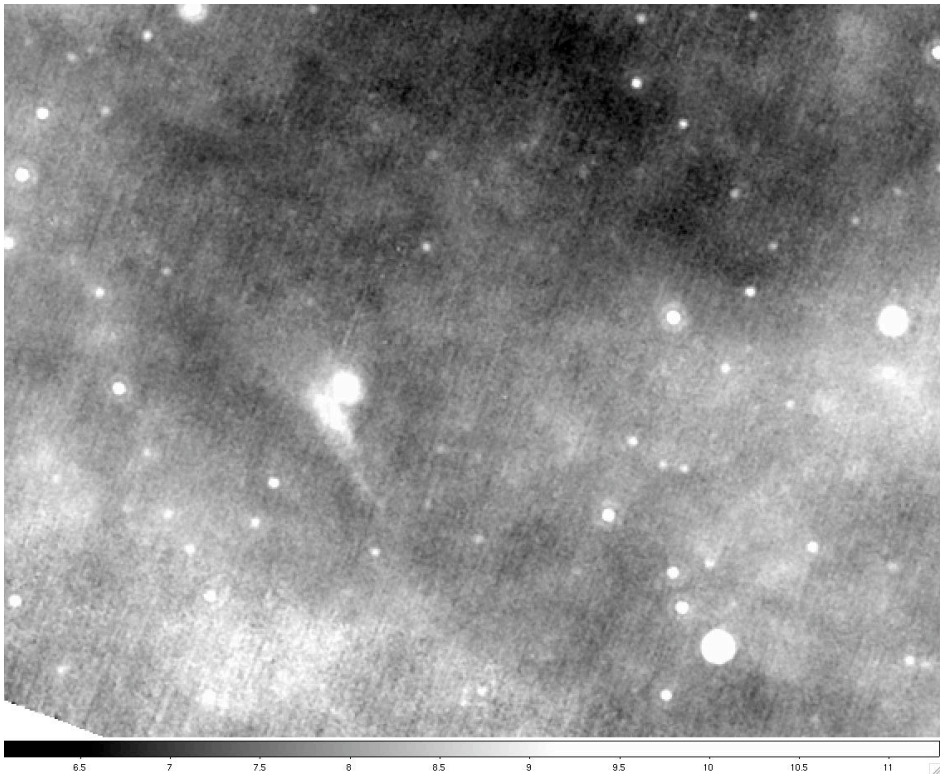

Figure 9: Subimage from the MG0640n005_024 plate displaying pattern noise.

Scan Edges

Small level jumps are present in some portions of the mosaics as shown in Figure 10. These discontinuities are at the scan boundaries between legs in an AOR or the boundary between AORs. Their impact on photometry should be minimal as they subtend a very small fraction of any given image.

Residual bright latents

The bright latent modeling and subtraction can leave noticeable residuals. Examples of residual latents are displayed in Figure 11. The residuals manifest themselves as bright or dark spots along the in-scan direction on either side of bright sources and will often look noisier than the surrounding data. In the worst cases, residuals can occur for up to three latent spots away from the bright source. These spots are equally spaced on either side of the latent producing source. However, most instances of latent residuals have been masked out when data scanned in the opposite direction is available.

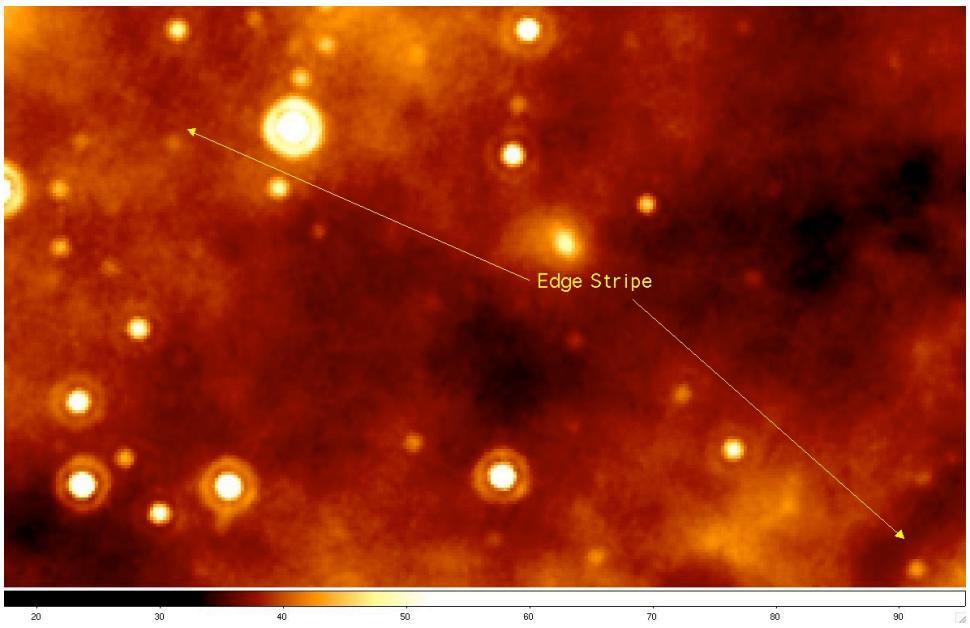

Figure 10: An example of a scan edge in the final mosaics.

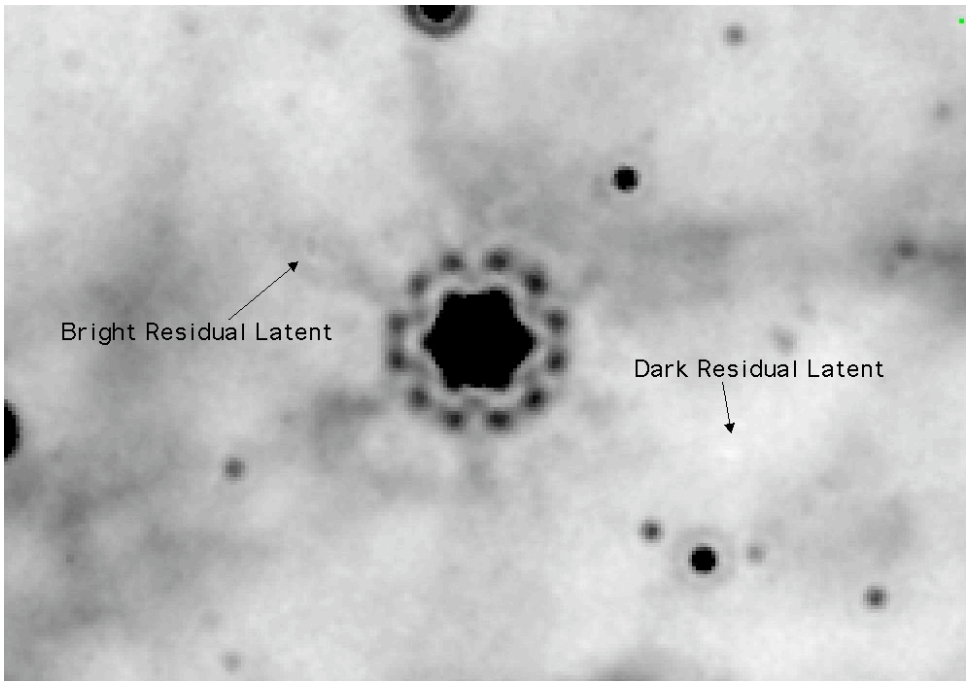

Figure 11: Examples of residual latents near on either side (in-scan direction) of a point source.

Dark latents

Dark latents are depressions in the pixel bias level created by very bright sources (>25 Jy; 362 such sources are present in these mosaics) imaged on the array. Figure 12 displays dark latents in MIPSGAL data prior to artifact mitigation. The latents persist until the array is annealed, which occurred approximately every 12 hours for the MIPSGAL data. However, we removed the dark latents from each AOR by identifying dark latents in the BCD stacks and correcting with an additive offset. Dark latents produced by sources in an AOR were identified by tracking known bright sources as well as a visual inspection of each BCD stack. Despite the care taken in removing dark latents, a few persist in the final mosaics. The latents are usually circular in appearance and will be spaced ~72 arcseconds apart in the in-scan direction (as that is the spacing between sequential pointings in MIPS fast scan data).

Extended bright latents

Latent images from extremely bright extended sources containing saturated pixels are not corrected in the MIPSGAL pipeline. For point sources, the pipeline estimates the surface brightness of saturated triggering pixels by fitting the unsaturated Airy rings of the source. This technique is not feasible for saturated extended structures. Most extended bright latents are mitigated in the mosaics by outlier rejection. However, the outlier rejection does leave residuals and extended latents will not be mitigated for areas without scan coverage in both directions. As shown in Figure 13, the residual extended latents can appear as faint rings spaced in 72 arcsecond increments above or below the source in the in-scan direction. Users should be cautious of ringlike morphologies near regions containing a cluster of saturated pixels.

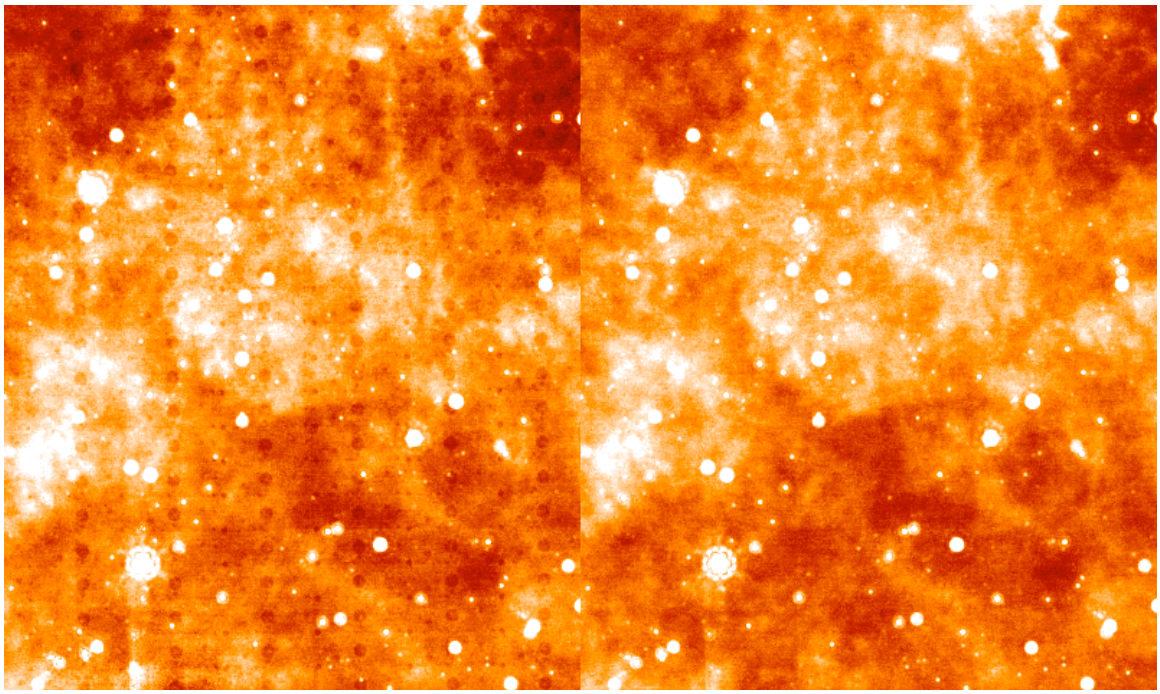

Figure 12: On the left is a mosaic produced without dark latent correction. The right is the same data with the dark latent correction applied.

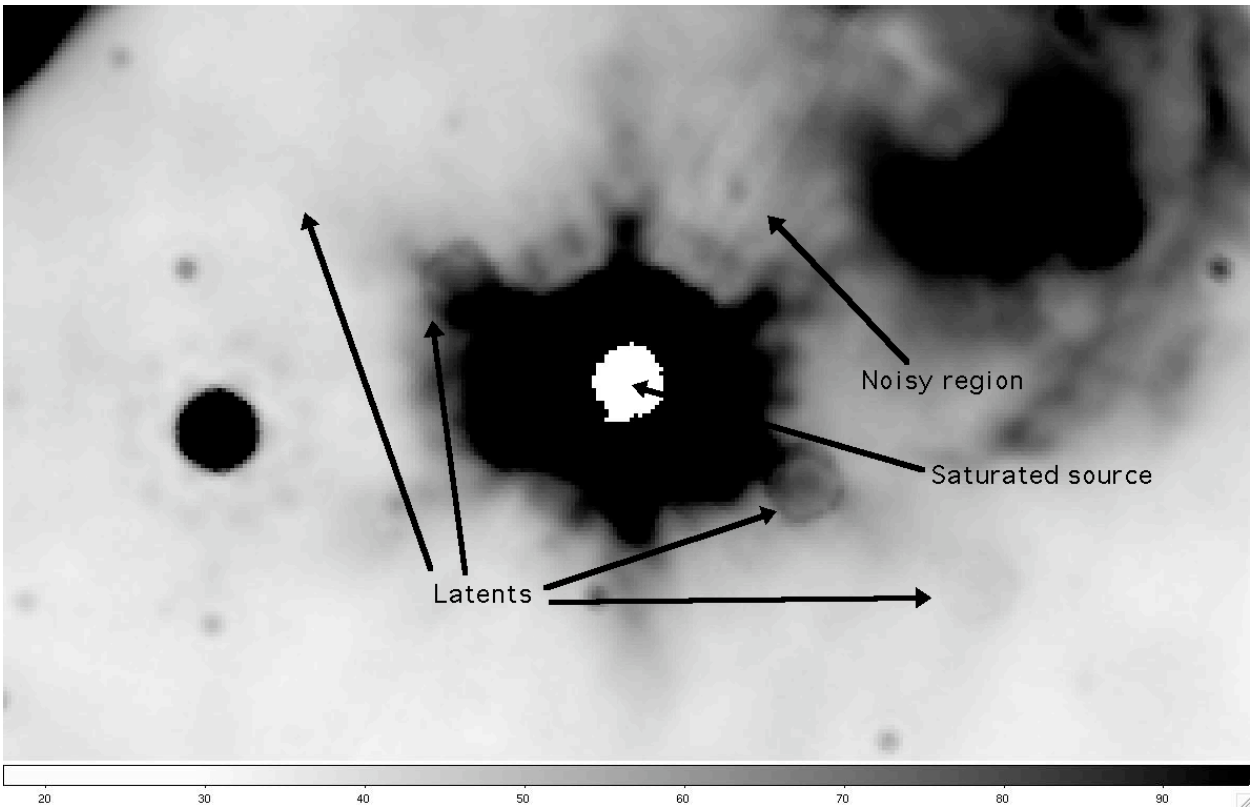

Figure 13: Example of mosaic artifacts produced by a saturated extended source. Bright latents exist in the in-scan direction and a noisy region remain in cross-scan.

Stray light

Stray light from bright sources off the array have been masked in the majority of cases. Some instances of stray light may have been missed in the interactive masking process and may be present in the final mosaics. Figures 13 and 14 show examples of stray light from bright and extremely bright (> 10 Jy) sources, respectively, that users of the data should be aware of. In both figures, the peak of the stray-light producing source is just off the array.

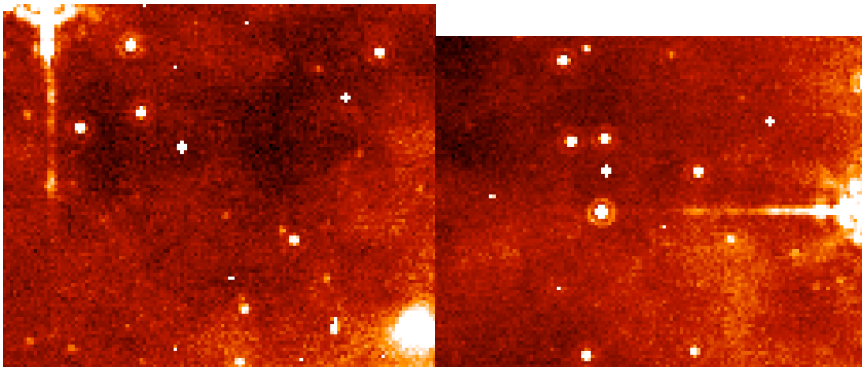

Figure 14: Two examples of streaks of stray light in BCD images. The width of each image is 5 arcminutes.

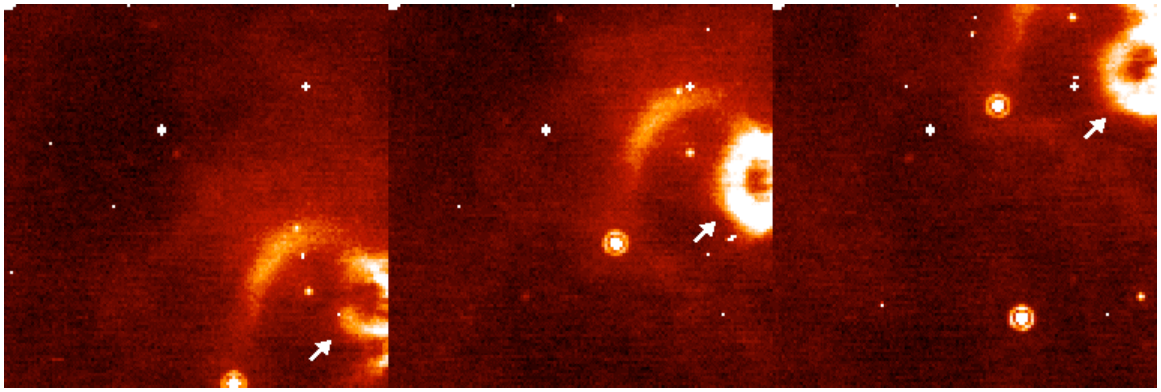

Figure 15: Examples of loops of stray light from very bright (> 10Jy) source. The left, middle and right panels are successive BCDs in a scan.

Noisy regions near bright sources

In some instances, the jailbar pattern and the cross-scan discontinuity in the jailbars are incompletely corrected for some sources. Near those sources are regions of higher noise extending on either side of the source in the cross-scan direction. The noisy region can have a total extent of 5 arcminutes in cross-scan and is usually less than the 2nd Airy ring in length (~48 arcsec) in the in-scan direction. For saturated extended sources, the noisy region can have a greater in-scan extent (as shown in Figure 8).

References

Calabretta, M. R., & Greisen, E. W. 2002, A&A, 395, 1077
Cohen, M. et al. 2003, AJ, 125, 2645
Engelbracht, C. W. et al. 2007, arXiv:0704.2196
Engelke, C. et al. 2006, AJ, 132, 1445
Kelsall, T. et al. 1998, ApJ, 508, 44
Laine, S. et al. 2006, IRAC Data Handbook, http://ssc.spitzer.caltech.edu/irac/dh/
Makovoz, D. et al. 2006, Proceedings of the SPIE, 6065, 330
Makovoz, D., & Marleau, F. 2005, PASP, 836, 1113
Malkov, O. Yu., et al. 2006, A&A, 446, 785
Meixner, M. 2006, The SAGE Data Description: Delivery 1, http://data.spitzer.caltech.edu/popular/sage/SAGE_SSCdatadocument_delivered.pdf
Mizuno, D. R., et al. 2008, in preparation
Rieke, G. H. et al. 2004, ApJS, 154, 25
Werner, M. et al. 2004, ApJS, 154, 1

Sample mosaic header

The following header is for the 24 μm mosaic centered on $l = 64°$, $b = -0.5°$

```
------- FITS file={../afrl_v1.1/MG0640n005_024.fits}
1234567890123456789012345678901234567890123456789012345678901234567890123456789
BITPIX  =                  -32 / Bits per pixel- floating point
NAXIS   =                    2 / STANDARD FITS FORMAT
NAXIS1  =                 3168
NAXIS2  =                 3168
TELESCOP= 'Spitzer '           / Spitzer Space Telescope
INSTRUME= 'MIPS    '           / Spitzer Space Telescope instrument ID
CHNLNUM =                    1 / This image: 1=24um,2=70um,3=160um
WAVELENG=          2.36800E-05 / [m] Isophotal wavelength of bandpass
PROGID  =                20597 / Program ID
PROGRAM = 'MIPSGAL '           / A 24 & 70 um Survey of the Inner Galactic Disk
OBSRVR  = 'Sean Carey'         / PI
PROGID2 =                30592 / Program ID of extended survey MIPSGAL2
FILENAME= 'MG0640n005_024.fits' / Name of this file
LPLATE  =                 64.0 / [deg] glon at plate center
BPLATE  =                 -0.5 / [deg] glat at plate center
DATE_OBS= '2005-10-08T11:12:58.556' / Date & time at DCE start
CRVAL1  =             298.7028 / [deg] RA at CRPIX1,CRPIX2
CRVAL2  =              27.0834 / [deg] DEC at CRPIX1,CRPIX2
RADESYS = 'ICRS    '           / International Celestial Reference System
EQUINOX =                2000. / Equinox for ICRS celestial coord. system
CTYPE1  = 'RA---TAN'           / RA projection type
CTYPE2  = 'DEC--TAN'           / DEC projection type
CRPIX1  =          1584.498901
CRPIX2  =          1584.498901
CDELT1  =         -0.000347222 / [deg/pix] Scale for axis 1
CDELT2  =          0.000347222 / [deg/pix] Scale for axis 2
CROTA2  =             58.89387 / [deg] Orientation of axis 2 (W of N, +=CW)
COMMENT Equatorial coordinate system is chosen to mimic
COMMENT the Galactic coordinate orientation.
BUNIT   = 'MJy/sr  '           / Units of image data
DATAMIN =              5.72979 / [MJy/sr] Minimum pixel value
DATAMAX =              2489.28 / [MJy/sr] Maximum pixel value
COVRGMN =              8.87093 / mean # of BCDs/pixel
COVRGMAX=                   21 / maximum # of BCDs/pixel
```

```
COVRGMIN=                    1 / minimum # (>0) of BCDs/pixel
NCOVRGE0=              1788700 / pixels with no coverage
PCOVRGE0=              17.8224 / [%] pixels with no coverage
PHARDSAT=           0.00160419 / [%] pixels flagged as hard saturated
NHARDALL=              1788773 / # pixels with all BCDs hard sat'd
PSOFTSAT=           0.00800102 / [%] pixels flagged as soft saturated
NSOFTALL=              1788774 / # pixels with all BCDs soft sat'd
EXPTIME =              2.62000 / [sec] t_int per pixel per BCD
MEANEXP =              28.2556 / [sec] mean t_int per pixel
GAIN    =                    5 / e/DN conversion
FLUXCONV=            0.0447000 / DN/s to MJy/sr factor
COMMENT MOSAIC_INT Module Version 5.3 image created
COMMENT Fri Apr 27 04:30:53 2007
COMMENT MOSAIC_REINT Module Version 2.7 image created
COMMENT Fri Apr 27 08:03:52 2007
COMMENT MOSAIC_COADD Module Version 3.5 image created
COMMENT Fri Apr 27 08:49:11 2007
COMMENT MOSAIC_COMBINE Module Version 1.9 image created
COMMENT Fri Apr 27 08:49:29 2007
TOTALBCD=                 1722 / Total number of BCD's used in this mosaic
BCDLIST = 'MG0640n005_024.bcdlist' / file containing list of BCDs
DROOP   =                    T / Droop Correction Applied
OVERLAP =                    T / Overlap Correction Applied
JAILBAR =                    T / Jailbar Correction Applied
DARKLAT =                    T / Dark Latent Correction Applied
WASHBRD =                    T / Washboard Correction Applied
BRITELAT=                    T / Bright Latent Correction Applied
EDGEMASK=                    T / Edge-source Masking Applied
ASTRDMSK=                    T / Asteroid Masking Applied
HISTORY Pre-mopex processing MIPSGAL BCD pipeline 1.0
HISTORY and Artifact Correction pipeline 1.0; see Carey et al. 2007
HISTORY and Mizuno et al. 2007, respectively, for details.
HISTORY Zodiacal background estimate, included by the SSC in the BCDs &
HISTORY based on the DIRBE model, is subtracted at the BCD level.
HISTORY Delivery V1.1b
NAORS   =                    9 / # of AORS used in mosaic
AORKEY00=             15576832 / Astronomical Observation Request Key Number
AORTIM00= '2005-10-08T10:37:28.379' / AOR Start Time
AORKEY01=             15579648 / Astronomical Observation Request Key Number
AORTIM01= '2005-10-08T11:53:38.583' / AOR Start Time
AORKEY02=             15598336 / Astronomical Observation Request Key Number
AORTIM02= '2005-10-09T00:53:25.352' / AOR Start Time
AORKEY03=             15618304 / Astronomical Observation Request Key Number
AORTIM03= '2005-10-08T20:57:57.413' / AOR Start Time
AORKEY04=             15638784 / Astronomical Observation Request Key Number
AORTIM04= '2005-10-08T18:18:43.874' / AOR Start Time
AORKEY05=             15639296 / Astronomical Observation Request Key Number
AORTIM05= '2005-10-08T19:41:45.116' / AOR Start Time
AORKEY06=             15650304 / Astronomical Observation Request Key Number
AORTIM06= '2005-10-08T23:37:13.054' / AOR Start Time
AORKEY07=             15651072 / Astronomical Observation Request Key Number
AORTIM07= '2005-10-08T13:09:50.880' / AOR Start Time
AORKEY08=             15663104 / Astronomical Observation Request Key Number
AORTIM08= '2005-10-08T22:20:58.659' / AOR Start Time
VERSION =              1.10000 / Version of 24 micron mosaic
-------
```